Greedy MRI reconstruction using Markov Random Field prior

Marko Panić*, Dejan Vukobratovic†, Vladimir Crnojević* and Aleksandra Pižurica‡
*University of Novi Sad, BioSense Institute
mpanic@uns.ac.rs, crnjvc@gmail.
†University of Novi Sad, Department of Power, Electronics and Telecommunications
dejan.vukobratovic@gmail.com
‡Ghent University, Department Telecommunications and Information Processing, TELIN-IPI-iMinds
Aleksandra.Pizurica@ugent.be

***Abstract*—Recent work on compressed sensing in magnetic resonance imaging (CS-MRI) indicates benefits of modelling the *structure* of sparse coefficients. Comprehensive studies are available for tree-structured models. Much less work has been done on using statistical models for intra-scale (spatial) dependencies, like Markov Random Field (MRF) models in CS-MRI, although initial studies showed great potentials. We present here an efficient greedy algorithm with MRF priors and demonstrate encouraging performance in comparison to related methods, including those based on tree-structured sparsity.**

I. Introduction

Compressed sensing (CS) for magnetic resonance imaging (MRI), dubbed CS-MRI, typically solves the problem

$$\min_{\mathbf{x}} \frac{1}{2}||\mathbf{A}\mathbf{x}-\mathbf{y}||_2^2 + \tau\phi(\mathbf{P}\mathbf{x}) \tag{1}$$

where $\mathbf{x} \in \mathbb{C}^N$ is the ideal image and $\mathbf{y} \in \mathbb{C}^M$ are measurements obtained through partially observed Fourier transform $\mathbf{A} \in \mathbb{C}^{M\times N}, M \ll N$, with added noise $\mathbf{n} \in \mathbb{C}^M$ [1], [2]. $\mathbf{P} \in \mathbb{C}^{D\times N}$ denotes a sparsifying transform, $\tau > 0$ is a parameter and $\phi : \mathbb{C}^D \mapsto \mathbb{R} \cup \{-\infty, +\infty\}$ is a regularization function. When $\mathbf{P}$ is a wavelet-like transform, ϕ is typically the ℓ_1 norm: $\phi(\boldsymbol{\theta}) = ||\boldsymbol{\theta}||_1$. An improved iterative solver with a usage of tight frames such as contourlets, shift-invariant discrete wavelet (SIDWT) and patch based directional wavelet (PBDW) and ℓ_1 norm regularization is reported in [3]. Another common regularization is Total Variation (TV), where $\mathbf{P}$ is a discrete gradient operator. Compound regularization (a combination of ℓ_1 and TV) is often used as well [1], [2], [4], [5]. Recent works incorporate modelling the *structured sparsity*, and in particular wavelet tree models have been proved beneficial in CS-MRI [6], [7]. An elegant algorithm LaMP (Lattice Matching Pursuit), which incorporates modelling of the spatial support of sparse images by a Markov Random Field (MRF), into a greedy solver was introduced in [8]. LaMP is not directly applicable to images that are not sparse in the canonical domain (and most MRI images are not). A related algorithm LaSB (Lattice Split Bregman) [9], which combines MRF modelling of the subband data with an augmented Lagrangian method showed promising results in MRI. It was unclear so far whether the success of LaSB could also be reached with a simpler, greedy type of methods, and it was also not clear how any of these methods would compare to alternative wavelet-tree sparsity methods [6], [7]. We address these questions and design a fast and simple MRF-based method for CS-MRI, demonstrating excellent performance.

A preliminary version of this work has been reported as an abstract only, in [10]. Here we elaborate the method, explaining the details of the algorithm and we provide for the first time its thorough analysis and evaluation on real MRI images. This work complements our recently reported alternative method based on optimisation theory [11]. Our new algorithm, proposed in this paper is conceptually much simpler and easier to implement and analyse compared to [11], while it provides similar improvement over the state-of-the-art wavelet-tree sparsity methods.

II. A greedy CS-MRI algorithm with MRF priors

Let us first revisit briefly the original Lattice Matching Pursuit (LaMP) algorithm of [8], before analysing possible extensions to make it applicable to MRI. Our new algorithm, inspired by this analysis, will follow then.

The original LaMP, with the pseudocode (using our notation) in Alg. 1, assumes that the image is sparse in the canonical domain. Its main idea is to incorporate the estimation of the likely *support* $\mathbf{s}$ of the actual signal into the matching pursuit iterations. They utilized a MRF prior or equivalently, according to the Hammersley-Clifford theorem [12], a Gibbs distribution $P_{\mathbf{S}}(\mathbf{s})$ for a *support* $\mathbf{s}$

$$P_{\mathbf{S}}(\mathbf{s}) = \frac{1}{Z}e^{-H(\mathbf{s})/T} \tag{2}$$

where the energy $H(\mathbf{s})$ is a sum of clique potentials over all possible cliques: $H(\mathbf{s}) = \sum_{c\in\mathcal{C}} V_c(\mathbf{s})$. The normalizing constant $Z = \sum_{\mathbf{s}\in\mathcal{L}} e^{-H(\mathbf{s})/T}$ is called the partition function and the temperature T controls the peaking in the probability density [12]. For an energy $H(\mathbf{s})$ an Ising model defined on a rectangular lattice with labels $s_i \in \{-1, 1\}$ is used, with the single $V_1(s_i) = \alpha s_i$ and pairwise $V_2(s_i, s_j) = \beta s_i s_j$ potentials

$$H(\mathbf{s}) = \sum_i \alpha s_i + \sum_{\langle i,j\rangle\in\mathcal{C}} \beta s_i s_j \tag{3}$$

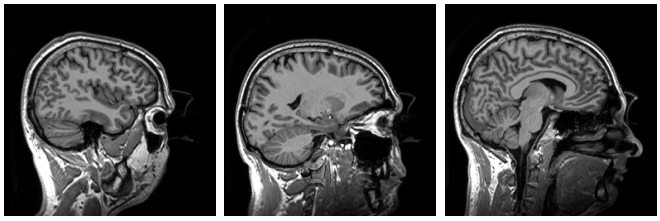

Fig. 1. Several sagittal slices from our MRI data set comprising 248 slices.

where β and α are the parameters of the Ising model, controlling the strength of the pair-wise clique potentials and the preference of one type of labels over the other, respectively.[1] In particular, Step 4 in each iteration k of Alg. 1 assigns to $\mathbf{s}^{\{k\}}$ the *maximum a posteriori* (MAP) estimate of the support of the temporary signal estimate $\mathbf{x}_t^{\{k\}}$, assuming a MRF prior $P_{\mathbf{S}}(\mathbf{s})$ for the support. With a homogeneous Ising model and using the common conditional independence assumption for the likelihood $p(\mathbf{x}_t|\mathbf{s}) = \prod_i p([\mathbf{x}_t]_i|s_i)$, the MAP estimate of the support of $\mathbf{x}_t^{\{k\}}$ (denoted as *MAP-support*$\{\mathbf{x}_t^{\{k\}}\}$ in Alg. 1) is:

$$\mathbf{s}_{MAP}^{\{k\}} = \max_{\mathbf{s}\in[-1,1]^N} \sum_{\langle i,j\rangle} \beta s_i s_j + \sum_i [\alpha s_i + \log(p([\mathbf{x}_t^{\{k\}}]_i|s_i)]$$

The pseudo-inversion $\mathbf{A}^\dagger$ of the measurement matrix (Step 5) is then applied only for the columns of $\mathbf{A}$ selected by $\mathbf{s}^{\{k\}}$. Additional pruning to K largest signal components (Step 6) yields the signal estimate $\mathbf{x}^{\{k\}}$.

This algorithm is directly applicable to the problem (1), only with $\mathbf{P} = \mathbf{I}$, where $\mathbf{I}$ is the identity matrix. We need to extend it such that it works in the case where $\mathbf{P}$ corresponds to a wavelet-like transform. A possible extension, which would allow applying LaMP to CS-MRI would be to replace steps 4-6 with:

$$\boldsymbol{\theta}_t^{\{k\}} = \mathbf{P}\mathbf{x}_t^{\{k\}}; \quad \mathbf{s}^{\{k\}} = \textit{MAP-support}\{\boldsymbol{\theta}_t^{\{k\}}\} \tag{4a}$$

$$\boldsymbol{\theta}_{t'}^{\{k\}} = \mathbf{P}\mathbf{A}^\dagger\mathbf{y}; \quad \mathbf{t}[\mathbf{s}^{\{k\}} = 1] = \boldsymbol{\theta}_{t'}^{\{k\}}[\mathbf{s}^{\{k\}} = 1] \tag{4b}$$

$$\boldsymbol{\theta}^{\{k\}} = \textit{Prune}(\mathbf{t}, K); \quad \mathbf{x}^{\{k\}} = \mathbf{P}^H\boldsymbol{\theta}^{\{k\}} \tag{4c}$$

Two important problems with this extension are: (i) the calculation of $\mathbf{P}\mathbf{A}^\dagger\mathbf{y}$ is costly, both in terms of the computation time and memory requirements and (ii) determining K in each subband is not trivial. Hence, we propose a simplified, greedy algorithm where the computation of the pseudo inverse is avoided by replacing $\boldsymbol{\theta}_{t'}^{\{k\}}$ in (4b) by $\boldsymbol{\theta}_t^{\{k\}}$ and by excluding the additional pruning step (4c) (the sparseness is guaranteed already by the estimated support $\mathbf{s}^{\{k\}}$ using the right parameters of the prior MRF model). Unlike in [9], we allow different a priori probabilities $\alpha \neq 0$, so that we can enforce the sparsity of the supports.

The proposed greedy algorithm named GreeLa (Greedy Lattice regularization) is summarized in Alg. 2. We employ the likelihood model from [9]. Various inference algorithms

[1] In [8], a *non-homogeneous model* is allowed, with variable parameters $\beta_{i,j}$ and α_i depending on the spatial position, but this is not relevant here.

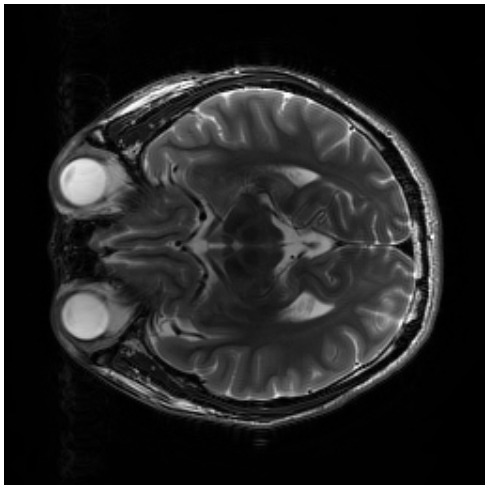

Fig. 2. An MRI image from [3].

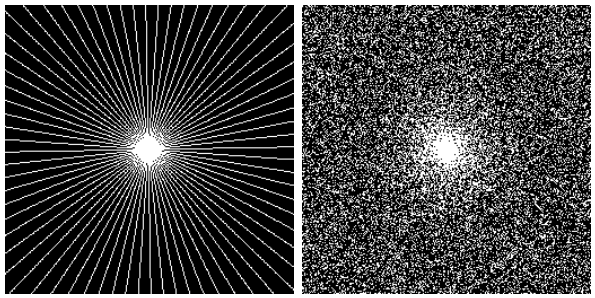

Fig. 3. Examples of sampling trajectories used in our experiments. **Left**: radial. **Right**: random.

can be utilized to find the MAP estimate in step 5 of GreeLa, e.g., Iterative Conditional Modes (ICM) [13], Graph Cuts [14], loopy belief propabation (LBP) [15], and Markov Chain Monte Carlo (MCMC) samplers, such as Metropolis and Gibbs sampler [12]. We opted for the Metropolis sampler due to its flexibility and efficiency in this application. The Metropolis sampler starts from some initial configuration and in each step it switches a randomly chosen label s_i in the current mask $\mathbf{s}$ to produce the so-called "candidate" mask $\mathbf{s}^C$. The candidate gets accepted or not based on the change in the posterior probability $P_{\mathbf{S}|\boldsymbol{\Theta}}(\mathbf{s}^C|\boldsymbol{\theta})/P_{\mathbf{S}|\boldsymbol{\Theta}}(\mathbf{s}|\boldsymbol{\theta})$, which effectively reduces to

$$r = \left(\frac{p_{\theta_i|S_i}(\theta_i \mid s_i^C = 1)}{p_{\theta_i|S_i}(\theta_i \mid s_i = -1)}\right)^\lambda \exp\left\{2\alpha + 2\beta \sum_{j\in\mathcal{N}_i} 2s_j\right\} \tag{5}$$

when $s_i^C = 1$ and to $1/r$ when $s_i^C = -1$. Practically, the change is accepted if r exceeds a randomly generated number drawn from a uniform distribution on $[0, 1]$. Parameter $\lambda > 0$ effectively simulates sampling at different temperatures; for details see [16]. This inference algorithm is in fact a step of the simulated annealing algorithm from [17] for a particular temperature — one could apply simulated annealing by changing gradually λ although we didn't do it in our experiments. Although there is no theoretical guarantee for

Algorithm 1 LaMP [8]

Input: $k = 1, \mathbf{y}, K, \mathbf{x}^{\{0\}}, \mathbf{t} = \mathbf{0}$

repeat{Matching Pursuit Iterations}
  $\mathbf{r}^{\{k\}} = \mathbf{y} - \mathbf{A}\mathbf{x}^{\{k-1\}}$
  $\mathbf{x}_t^{\{k\}} = \mathbf{A}^H \mathbf{r}^{\{k\}} + \mathbf{x}^{\{k-1\}}$
  $\mathbf{s}^{\{k\}} = \textit{MAP-support}\{\mathbf{x}_t^{\{k\}}\}$
  $\mathbf{t} = \mathbf{0}; \quad \mathbf{t}[\mathbf{s}^{\{k\}} = 1] = \mathbf{A}^{\dagger}[\mathbf{s}^{\{k\}} = 1, :]\mathbf{y};$
  $\mathbf{x}^{\{k\}} = \textit{Prune}(\mathbf{t}, K)$
  $k = k + 1$
until Maximum iterations or $\|\mathbf{r}^{\{\mathbf{k}\}}\| \leq threshold$

Algorithm 2 The proposed algorithm: GreeLa

Input: $k = 1, \mathbf{y}, \mathbf{x}^{\{0\}}, \mathbf{t} = \mathbf{0}$

repeat
  $\mathbf{r}^{\{k\}} = \mathbf{y} - \mathbf{A}\mathbf{x}^{\{k-1\}}$
  $\mathbf{x}_t^{\{k\}} = \mathbf{A}^H \mathbf{r}^{\{k\}} + \mathbf{x}^{\{k-1\}}$
  $\boldsymbol{\theta}_t^{\{k\}} = \mathbf{P}\mathbf{x}_t^{\{k\}}$
  $\mathbf{s}^{\{k\}} = \textit{MAP-support}\{\boldsymbol{\theta}_t^{\{k\}}\}$
  $\mathbf{t} = \mathbf{0}; \quad \mathbf{t}[\mathbf{s}^{\{k\}} = 1] = \boldsymbol{\theta}_t^{\{k\}}[\mathbf{s}^{\{k\}} = 1]$
  $\boldsymbol{\theta}^{\{k\}} = \mathbf{t}, \mathbf{x}^{\{k\}} = \mathbf{P}^H \boldsymbol{\theta}^{\{k\}}$
  $k = k + 1$
until Maximum iterations or $\|\mathbf{r}^{\{\mathbf{k}\}}\| \leq threshold$

the convergence at this point, the proposed method converges in practice relatively fast.

III. Experiments and Discussion

Here we report the results of extensive experiments on different MRI images, including an MRI data set (brain scan) acquired on a Cartesian grid at the Ghent University hospital (UZ Gent)[2], also used in [9], [18]. We show the results on 248 sagittal slices from this data set (each slice is a 256×256 image, and in a Fig. 1 we show some of them). We provide results of comparison with the pFISTA method [3] on an image used in [3]. The results are reported for simulated *radial* and *random* undersampling trajectories in Fig. 3. For the sparsifying transform we used the non-decimated wavelet transform with 3 scales and with 3 orientations per scale (fine-to-coarse) in all our experiments. We compare the results to LaSB [9], and to state-of-the art methods FCSA [4], FCSANL [19] and WaTMRI [7] with the original implementations[3]. All these methods, except LaSB, employ a compound regularization. FCSA combines TV and ℓ_1 norms while FCSANL combines non-local TV and ℓ_1 norm. WaTMRI besides TV and ℓ_1 norm involves overlapping groups in regularization as a approximation of tree-structured sparsity. Finally we include results of image reconstruction of *pomelo* fruit from real radially acquired measurements provided by Bio-Imaging Lab in Antwerp. The MRF parameters were optimized separately for LaSB ($\alpha = .017$, $\beta = .07$) and for GreeLa ($\alpha = 1e-4$, $\beta = .34$) and such as are used in all presented results.

[2]Data acquired thanks to Prof. Dr. Karel Deblaere at the Radiology Department of UZ Gent.

[3]http://ranger.uta.edu/~huang/index.html

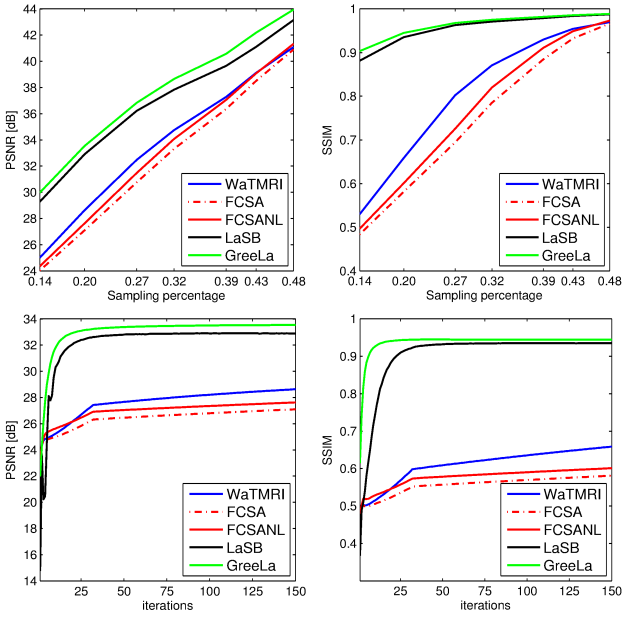

Fig. 4. **Top left** and **Top right**: PSNR and SSIM for the reconstructions of one slice (the second in Fig. 1) at different sampling rates. **Bottom left** and **Bottom right**: Reconstruction performances in PSNR and SSIM, respectively on the same slice with 20% measurements in 150 iterations.

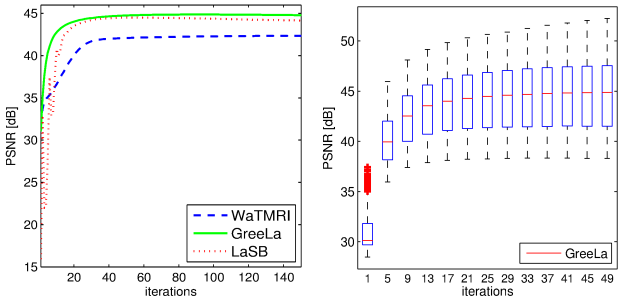

Fig. 5. PSNR values obtained from 248 MRI *brain slices* from the first data set, with radial sampling. Mean PSNR (**Left**) and the PSNR distribution for GreeLa (**Right**). The results are presented as a box plot: the edges of the each box represents 25^{th} and 75^{th} percentile while the central mark (red line) in the box is median. The whiskers extend to the most extreme PSNR values which are not considered outliers while outliers are plotted separately with red crosses.

Fig. 4 shows the Peak Signal to Noise Ratio (PSNR) and Structural Similarity Index (SSIM) for one slice (the second image in Fig. 1), with sampling rate (SR) ranging from 14% to 48%, and the evolution of the PSNR and SSIM per iteration for a particular SR (20%). The MRF-based methods GreeLa and LaSB achieve a consistent and significant improvement in PSNR (more than 4 dB) compared to WaTMRI, FCSA and FCSANL for all SR values, and they also approach convergence in fewer iterations. GreeLa yields slightly higher PSNR than LaSB and shows a more stable behaviour in the first 20 iterations (see bottom left in Fig. 4). In case of SSIM measure LaSB and GreeLa outperform compared methods significantly for all sampling rates (seethe top right diagram in Fig. 4). LaSB and GreeLa reached SSIM above 0.85 for all

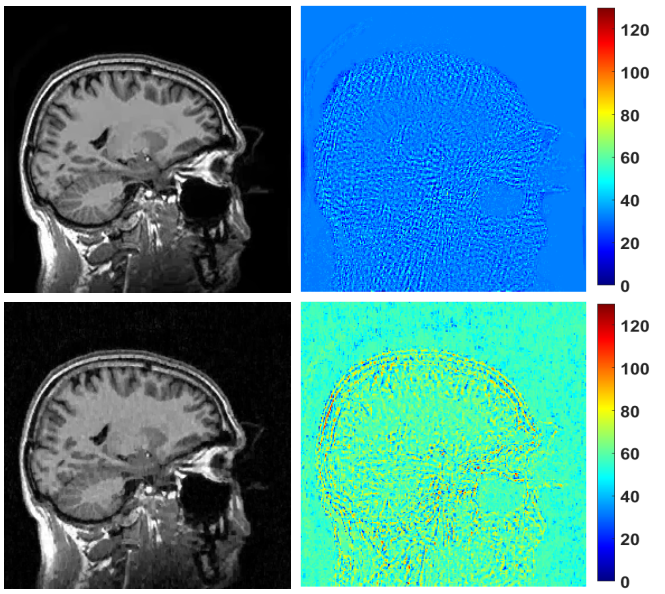

Fig. 6. Reconstructed image (the second in Fig. 1) from 20% of measurements using radial trajectory. **Top** GreeLa and **Bottom** WaTMRI algorithm. The images on the right show reconstruction errors.

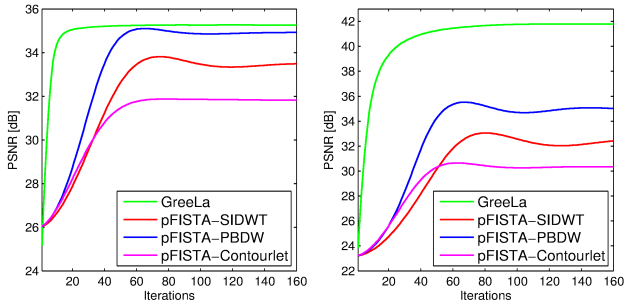

Fig. 7. PSNR for the reconstructions of the test image in Fig. 2 for different sampling trajectories. **Left**: radial and **Right**: random with the same sampling rate of 30%.

SR, GreeLa even more than 0.9 for a SR of 14%. For SR of 20%, LaSB and GreeLa reached the SSIM above 0.9 in less than 20 iterations (see bottom right in Fig. 4) while among the compared methods WaTMRI performed best with SSIM above 0.65 after 150 iterations. This significant structural difference in reconstruction for a low SR is presented in Fig. 6.

We show results of reconstruction of all 248 MRI sagittal slices from our dataset in Fig. 5 with SR=48%. Here we show only comparison with WaTMRI, since it outperforms FCSA and FCSANL on slices from this data set (see Fig. 4). The conclusions are as follows: although WaTMRI increased its performance on average, GreeLa and LaSB yield a superior PSNR and converge in fewer iterations. A more stable behaviour of GreeLa compared to LaSB and slightly better PSNR are again observed.

We next compared GreeLa with pFISTA [3] using the image from [3] (see Fig. 2). We now use random and radial sampling trajectory with the sampling rate of 30%. From the

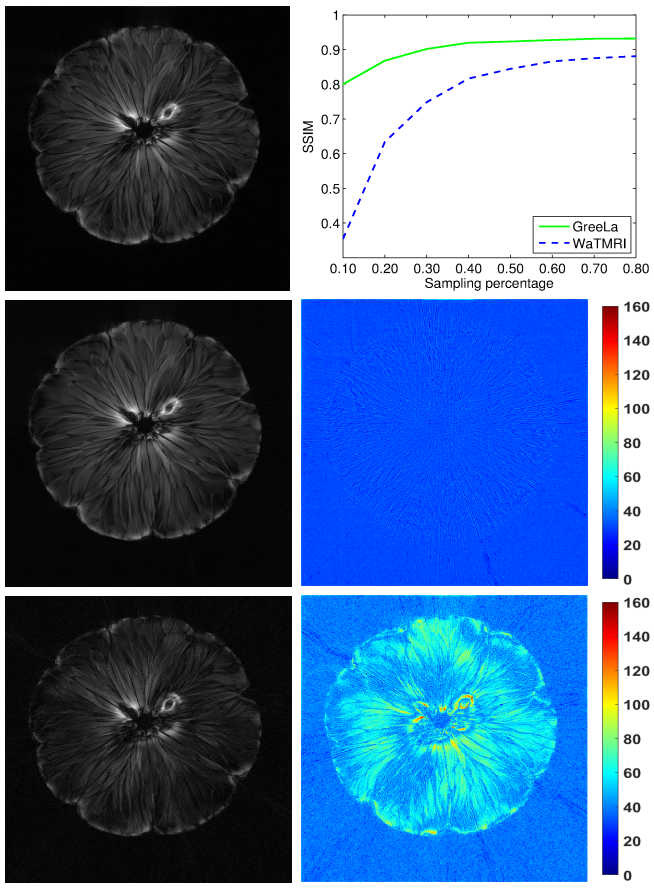

Fig. 8. Pomelo experiment. **The first column top to bottom**: reference image obtained from 100% of measurements, reconstructions from 20 % sampling rate using GreeLa and WaTMRI respectively. **The second column top to bottom**: Obtained SSIM for different sampling rates, followed by properly scaled error according to the corresponding reconstructions.

left diagram in Fig. 7 for the case of radial sampling trajectory, GreeLa reaches only slightly higher PSNR (35.3 dB) compared to the best version of pFISTA (35.1 dB). However, in the case of random sampling (the right-side diagram in Fig. 7), GreeLa yields a huge improvement of more than 6 dB compared to best performing pFISTA variant.

Next we perform experiments on a real MRI data set with radial acquisition in k-space. This is a scan of *pomelo*, acquired in the BioImaging Lab at the University of Antwerp (see Fig. 8). The data consist of 1608 radial lines, each with 1024 samples. We form under-sampled versions by leaving out some of the radial lines. In particular, we aim to implement undersampling based on the golden ratio profile spacing [20], which guarantees a nearly uniform coverage of the space for an arbitrary number of the remaining radial lines. Starting from an arbitrary selected radial line, each next line is chosen by skipping an azimuthal gap of $111.246°$. In practice we cannot always achieve this gap precisely (since we have a finite, although large, number of lines to start with). Therefore we choose the nearest available radial line relative to the position obtained after moving. Since we deal here with non-uniformly sampled k-space data, we need to employ the non-

uniform FFT procedures [20], which are commonly used in MRI reconstruction and readily available. In the reconstruction we include weights on non-uniform measurements based on an area of Voronoi cells around each sample point. In [21] is reported that using Voronoi weights as a measure of the local sampling density is very reliable. The three reference methods (WaTMRI, FCSA and FCSANL) give similar results on this image, so we choose for comparison WaTMRI. Fig. 8 shows visual comparison and SSIM values for GreeLa and WaTMRI. For all sampling rates, the proposed method GreeLa outperform WaTMRI. Given that the new algorithm is conceptually simpler, easier to implement and optimize, these results are highly encouraging.

IV. Conclusion

The presented work shows great potential of using MRF-based spatial context modelling in MRI reconstruction. The proposed algorithm GreeLa as an extension of the LaMP method for images that are non sparse in the canonical domain, outperforms state-of-the-art methods for MRI reconstructions and shows stable behaviour compared to the related MRF-based method LaSB. Moreover, significant improvements in the reconstruction performance are achieved compared to alternative methods based on wavelet-tree sparsity as well as compared to state-of-the-art method pFISTA. Additional complexity resulting from the MRF model is compensated by significant gains in terms of PSNR, SSIM and visual assessment.

References

[1] M. Lustig, D. Donoho, and J. M. Pauly, "Sparse MRI: The application of compressed sensing for rapid MR imaging," *Magnetic Resonance in Medicine*, vol. 58, no. 6, pp. 1182–1195, 2007.

[2] M. Lustig, D. L. Donoho, J. M. Santos, and J. M. Pauly, "Compressed sensing MRI," *IEEE Signal Processing Magazine*, vol. 25, no. 2, pp. 72–82, 2008.

[3] Y. Liu, Z. Zhan, J. Cai, D. Guo, Z. Chen, and X. Qu, "Projected iterative soft-thresholding algorithm for tight frames in compressed sensing magnetic resonance imaging," *IEEE Transactions on Medical Imaging*, vol. 35, no. 9, pp. 2130–2140, 2016.

[4] J. Huang, S. Zhang, and D. Metaxas, "Efficient MR image reconstruction for compressed MR imaging," *Medical Image Analysis*, vol. 15, no. 5, pp. 670–679, 2011.

[5] S. Ma, W. Yin, Y. Zhang, and A. Chakraborty, "An efficient algorithm for compressed MR imaging using total variation and wavelets," in *IEEE Conference on Computer Vision and Pattern Recognition (CVPR)*, 2008, pp. 1–8.

[6] C. Chen and J. Huang, "Compressive sensing MRI with wavelet tree sparsity," in *Advances in neural information processing systems*, 2012, pp. 1115–1123.

[7] C. Chen and J. Huang, "Exploiting the wavelet structure in compressed sensing MRI," *Magnetic Resonance Imaging*, vol. 32, no. 10, pp. 1377–1389, 2014.

[8] V. Cevher, M. F. Duarte, C. Hegde, and R. Baraniuk, "Sparse signal recovery using Markov random fields," in *Advances in Neural Information Processing Systems*, 2009, pp. 257–264.

[9] A. Pižurica, J. Aelterman, F. Bai, S. Vanloocke, Q. Luong, B. Goossens, and W. Philips, "On structured sparsity and selected applications in tomographic imaging," in *SPIE Conference on Wavelets and Sparsity XIV*, vol. 8138, 2011, pp. 81 381D–1–12.

[10] M. Panić, D. Vukobratović, V. Crnojević, and A. Pižurica, "Sparse MRI with a markov random field prior for the subband coefficients," in *Proceedings of the third "international Traveling Workshop on Interactions between Sparse models and Technology" (iTWIST'16)*, 2016, pp. 56–58. [Online]. Available: http://arxiv.org/abs/1609.04167

[11] M. Panić, J. Aelterman, V. Crnojević, and A. Pižurica, "Compressed sensing in MRI with a markov random field prior for spatial clustering of subband coefficients," in *24th European Signal Processing Conference, EUSIPCO 2016, Budapest, Hungary, August 29 - Sept. 2*, 2016.

[12] S. Z. Li, *Markov random field modeling in image analysis*. Springer Science & Business Media, 2009.

[13] J. Besag, "On the statistical analysis of dirty pictures," *Journal of the Royal Statistical Society. Series B (Methodological)*, pp. 259–302, 1986.

[14] V. Kolmogorov and R. Zabih, "What energy functions can be minimized via graph cuts ?" *IEEE Transactions on Pattern Analysis and Machine Intelligence*, vol. 26, pp. 65–81, 2004.

[15] K. P. Murphy, Y. Weiss, and M. I. Jordan, "Loopy belief propagation for approximate inference: An empirical study," in *Proceedings of the Fifteenth conference on Uncertainty in artificial intelligence*. Morgan Kaufmann Publishers Inc., 1999, pp. 467–475.

[16] A. Pizurica, W. Philips, I. Lemahieu, and M. Acheroy, "A joint inter-and intrascale statistical model for Bayesian wavelet based image denoising," *Image Processing, IEEE Transactions on*, vol. 11, no. 5, pp. 545–557, 2002.

[17] S. Kirkpatrick, "Optimization by simulated annealing: Quantitative studies," *J. Stat. Phys.*, vol. 34, no. 5-6, pp. 975–986, 1984.

[18] J. Aelterman, H. Q. Luong, B. Goossens, A. Pižurica, and W. Philips, "Augmented Lagrangian based reconstruction of non-uniformly sub-nyquist sampled MRI data," *Signal Processing*, vol. 91, no. 12, pp. 2731–2742, 2011.

[19] J. Huang and F. Yang, "Compressed magnetic resonance imaging based on wavelet sparsity and nonlocal total variation," in *Biomedical Imaging (ISBI), 2012 9th IEEE International Symposium on*. IEEE, 2012, pp. 968–971.

[20] S. Winkelmann, T. Schaeffter, T. Koehler, H. Eggers, and O. Doessel, "An optimal radial profile order based on the Golden Ratio for time-resolved MRI," *Medical Imaging, IEEE Transactions on*, vol. 26, no. 1, pp. 68–76, 2007.

[21] V. Rasche, R. Proksa, R. Sinkus, P. Bornert, and H. Eggers, "Resampling of data between arbitrary grids using convolution interpolation," *IEEE transactions on medical imaging*, vol. 18, no. 5, pp. 385–392, 1999.